

Electrical Spin Injection and Detection in Silicon Nanowires with Axial Doping Gradient

Konstantinos Kountouriotis,[†] Jorge L. Barreda,[†] Timothy D. Keiper,[†] Mei Zhang,[‡] and Peng Xiong^{*,†}

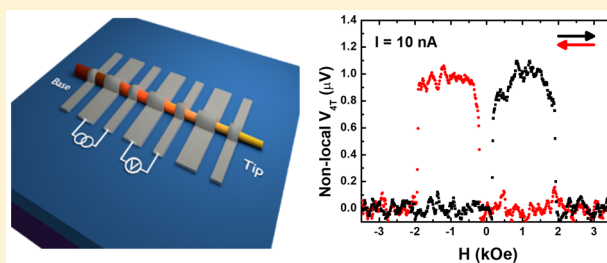
[†]Department of Physics, Florida State University, Tallahassee, Florida 32306, United States

[‡]Department of Industrial and Manufacturing Engineering, College of Engineering, Florida A&M University-Florida State University (FAMU-FSU), Tallahassee, Florida 32310, United States

S Supporting Information

ABSTRACT: The interest in spin transport in nanoscopic semiconductor channels is driven by both the inevitable miniaturization of spintronics devices toward nanoscale and the rich spin-dependent physics the quantum confinement engenders. For such studies, the all-important issue of the ferromagnet/semiconductor (FM/SC) interface becomes even more critical at nanoscale. Here we elucidate the effects of the FM/SC interface on electrical spin injection and detection at nanoscale dimensions, utilizing a unique type of Si nanowires (NWs) with an inherent axial doping gradient. Two-terminal and nonlocal four-terminal lateral spin-valve measurements were performed using different combinations from a series of FM contacts positioned along the same NW. The data are analyzed with a general model of spin accumulation in a normal channel under electrical spin injection from a FM, which reveals a distinct correlation of decreasing spin-valve signal with increasing injector junction resistance. The observation is attributed to the diminishing contribution of the d-electrons in the FM to the injected current spin polarization with increasing Schottky barrier width. The results demonstrate that there is a window of interface parameters for optimal spin injection efficiency and current spin polarization, which provides important design guidelines for nanospintronic devices with quasi-one-dimensional semiconductor channels.

KEYWORDS: Silicon nanowires, spin injection, spintronics, axial doping gradient, nano spin valves, Schottky barriers



Coherent spin transport and spin manipulation are two essential ingredients of semiconductor spintronic logic devices including several viable types of spin transistors, particularly spin field-effect transistors (FETs).^{1–5} The relevant research on spin injection and detection and spin coherence in semiconductors continues to draw extensive interest. Much progress has been made in bulk (thick films) semiconductors^{6–10} and more recently in the two-dimensional (2D) electron systems in semiconductor and oxide heterostructures.^{11–15} A number of critical issues have been addressed with significant enhancement in our understanding. The issue of efficient spin injection from a ferromagnet into a semiconductor, particularly the problem of “conductivity mismatch”, has seen in-depth theoretical^{16,17} and experimental^{9,10,13} studies. Several different approaches of interface engineering have been developed to optimize the spin injection efficiency;^{7,10,13,18,19} specifically, for FM metal injectors a large interface resistance is necessary for producing substantial current spin polarization in the semiconductor, whereas low-resistance Ohmic contacts invariably lead to low spin injection efficiency.

Microscopically, spin–orbit interactions (SOI) play important roles in spin FET devices, both as a means for spin manipulation via electric field^{1,11} and as a primary source of

spin decoherence.^{4,20} In this respect, semiconductor nanowires (NWs) may offer a distinct advantage over 2D and bulk semiconductors as the spin transport media due to effects from the one-dimensional (1D) confinement. It is proposed that by reducing the spin transport channel width, both the Elliot-Yafet (EY) and D'yakonov-Perel (DP) spin relaxation mechanisms can be suppressed, resulting in longer spin lifetime and spin diffusion length.^{21–23} The EY mechanism, being proportional to momentum relaxation, is suppressed because phonon scattering is reduced in NWs as a result of the reduced density of states of phonons. Experimentally, it was shown that the DP mechanism can be dimensionally constrained for widths as large as an order of magnitude larger than the electron mean free path.²⁴ For this reason and because of the eventual miniaturization of the spintronic devices down to nanoscales, there is great pertinent interest in the study of spin injection, detection, and coherent transport in 1D semiconductor nanostructures, particularly NWs.^{25–30}

Received: April 9, 2018

Revised: May 31, 2018

Published: June 13, 2018



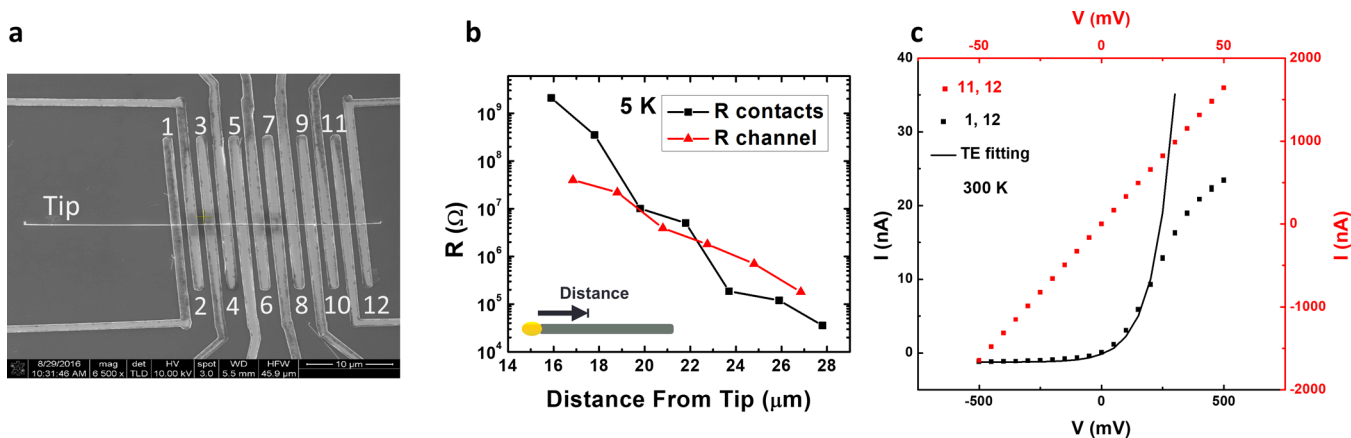


Figure 1. SEM micrograph and electrical characterizations of a CoFe/NW device. (a) SEM image of a Si NW device with CoFe electrodes. The numbering of the electrodes corresponds to the notation of the electrical measurements, which were performed in an identically designed device. (b) Contact and channel resistances with respect to the distance from the tip of the NW at 5 K, determined from combinations of 2T and 4T I - V measurements. (c) The 2T I - V curves from two different combinations of the most conducting electrode (#12) with the closest (#11, red) and furthest (#1, black) electrode on the same NW, which shows linear and rectifying behavior respectively at 300 K. The solid line represents the thermionic emission model fitting.

A variety of elemental and compound semiconductor NWs have been investigated based on the lateral spin valve geometry.^{31,32} Among these, silicon NWs have attracted particular attention because of their technological relevance and favorable spin-dependent physical characteristics. Over the years, spin transport measurements have been performed in bulk silicon^{33–39} and more recently on Si NWs. In comparison to the bulk and 2D systems, the NWs present particular difficulties in engineering the interface critical for spin injection and detection, both in terms of the NW morphology which tends to result in the “buckling” of the FM electrodes,²⁶ and the control of the interfacial electronic properties. For the former, different planarization methods have been employed²⁶ with varying degrees of success. For the latter, various oxides^{26,30} and graphene²⁷ were used as tunnel barriers to facilitate spin injection into the NWs. An approach widely employed in 2D devices, via engineering of a graded Schottky barrier (SB) at the FM metal/semiconductor interface which facilitates the formation of a thin tunneling barrier for efficient spin injection,⁴⁰ is not easily adaptable to the 1D cases. As a result, this highly effective approach has not been applied to semiconductor NW-based spin devices; in fact, there are few reports of NW spin devices utilizing SB contacts as spin injectors and detectors thus far.^{25–30}

In this work, we perform systematic spin transport measurements on a unique type of phosphorus-doped Si NWs which exhibit an inherent doping gradient along the axial direction. On a single NW, we place a series of FM electrodes, which form contacts that evolve from Ohmic-like to Schottky barriers of increasing heights/widths due to the doping gradient. Local two-terminal (2T) and nonlocal four-terminal (NL-4T) spin valve (SV) measurements using different combinations of FM electrodes positioned along the same NW thus facilitate a systematic examination of the dependence of the spin signal on the nature of the FM/SC nanointerface. The data reveal distinct correlations between the spin signals and the injector/detector interfacial properties. Significantly, while it is necessary to have a tunneling contact for efficient spin injection, increasing barrier width for the CoFe/Si-NW contacts, leads to decreasing injected current spin polarization due to diminishing contribution of the d-electrons; thus the

results demonstrate that there is an optimal window of interface parameters for maximum injected current spin polarization. We emphasize that the insights gleaned from the experiments were possible only because of the unique inhomogeneous doping profile in these NWs.

The silicon NWs used in this experiment are n-type phosphorus-doped, grown on SiO₂ substrates via the vapor–liquid–solid (VLS) deposition method. Details of the growth method are described previously.⁴¹ The Si NWs were dispersed onto a p⁺-doped Si substrate with SiO₂ (250 nm)/Si₃N₄ (50 nm) dielectric layers on top. Electron beam lithography was performed to define the electrode patterns on a selected NW. The native oxide on the NW surface was removed by a buffered HF etching, and Co₇₀Fe₃₀ (60 or 100 nm thick), followed by an Al capping layer (2 nm), was deposited by ultrahigh vacuum magnetron sputtering. The NWs were transferred immediately into an ultrahigh vacuum after the buffered HF etching. It is well accepted that the Si surface after such a buffered HF etch is hydrogen-passivated, which minimizes reoxidation of the Si. Therefore, we believe that in our devices there is minimal oxidation of the NW surface before the Co₇₀Fe₃₀ deposition, although the presence of small amount of SiO₂ cannot be completely ruled out. Several different electrode patterns were employed with different widths (0.8–1.2 μm) and separations (0.5–1.3 μm). Two electrode patterns were employed: one was used for basic characterizations with CoFe electrodes of the same width (1.0 μm) and separation (0.5 μm) and the other had alternating widths of 0.8 and 1.2 μm in order to obtain different coercive fields owing to shape anisotropy. For the latter, the electrode separation was kept between 0.8 and 1.8 μm , and Co₇₀Fe₃₀ thickness of 60 or 100 nm was used.

The axial doping gradient in these Si NWs stems from simultaneous fast VLS axial growth and slow vapor–solid (VS) radial growth, resulting in a core–shell structure.^{42–44} The much slower VS growth rate leads to much higher density of dopant incorporation for the shell and a variation of its thickness along the length of the NW and thus the axial doping gradient. The tapered geometry for the NWs is evident in the SEM images in Figure S1b,c. Electrically, we have demonstrated previously that by placing a series of Cr/Ag electrodes

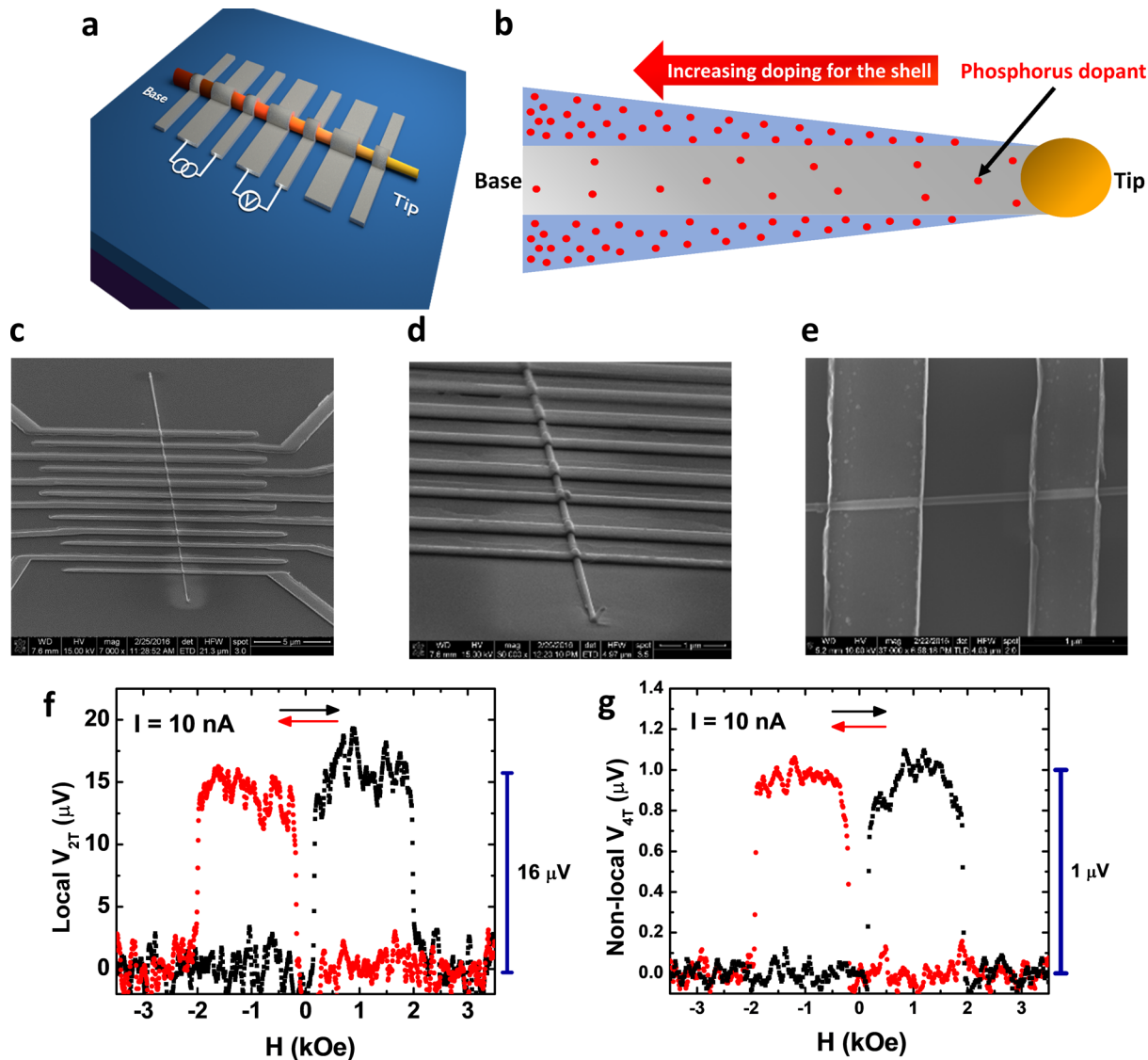


Figure 2. Schematic diagram, SEM micrographs and spin valve signals from a Si NW device. (a) Schematic diagram of a Si NW device in the nonlocal 4T spin valve setup. (b) Si NW schematic depicting the inhomogeneous phosphorus doping profile along the length of the NW. The red dots represent the phosphorus dopants. (c,d) SEM micrographs of a Si NW spin valve device. (e) SEM micrograph of two consecutive CoFe electrodes of different widths, 1.17 μm and 800 nm. (f,g) Local 2T and nonlocal 4T spin valve signals for the same Si NW channel at current bias $I = 10$ nA. The background has been subtracted.

along such a NW, one can obtain metal/NW contacts which evolve systematically from Ohmic to ideal Schottky.⁴⁵ Here we first verify that a similar evolution from linear to rectifying contacts can be obtained by using the FM $\text{Co}_{70}\text{Fe}_{30}$. Figure 1a shows an SEM image of a device used for the basic electrical characterizations of the NW and contacts. Combinations of 2T and 4T I - V measurements yield the zero-bias resistances of the contacts (R_j) and sections of the Si NW channel (R_{ch}) at different distances from the NW tip. Figure 1b shows the results at 5 K; it is evident that both R_j and R_{ch} vary exponentially along the NW, consistent with the results obtained in devices with nonmagnetic electrodes.⁴⁵ The resistivity from the base toward the tip as determined from the 4T measurements for the first eight segments changes from 0.009 to 0.027 $\Omega\text{-cm}$, which in comparison to bulk Si (at 300 K) corresponds to an effective carrier concentration change between 4.5×10^{18} and $6.8 \times 10^{17} \text{ cm}^{-3}$. This indicates a transition from a moderately doped to a low-doped regime.

Figure S2a shows R_j and R_{ch} along the NW at 300 K. At approximately 16 μm from the tip, there is a transition from a SB-dominated behavior to channel-limited Ohmic behavior indicated by the crossing of the two curves. Corresponding to the resistance variations, the 2T I - V evolves from linear at the base of the NW to rectifying closer to the tip (Figure 1c). The rectifying I - V at 300 K in Figure 1c is analyzed in the thermionic emission model and found to be consistent with that of an ideal Schottky junction. The extracted values for the Schottky barrier height, serial resistance and ideality factor are $\phi_B = 0.453 \text{ eV}$, $R_S \approx 12.7 \text{ M}\Omega$ and $n = 1$, respectively. We note that the deviation of the theoretical curve from the experimental data at high voltage biases is due to the pinch-off of the channel. In Figure S2d,e, we plot the semilog I - V curves for 300 and 5 K respectively for the 12 consecutive contacts; in Figure S3a-f, three sets of the I - V curves are plotted on linear scales. It is evident that at 5 K, the rectifying I - V curves at 300 K become symmetric, suggesting that the

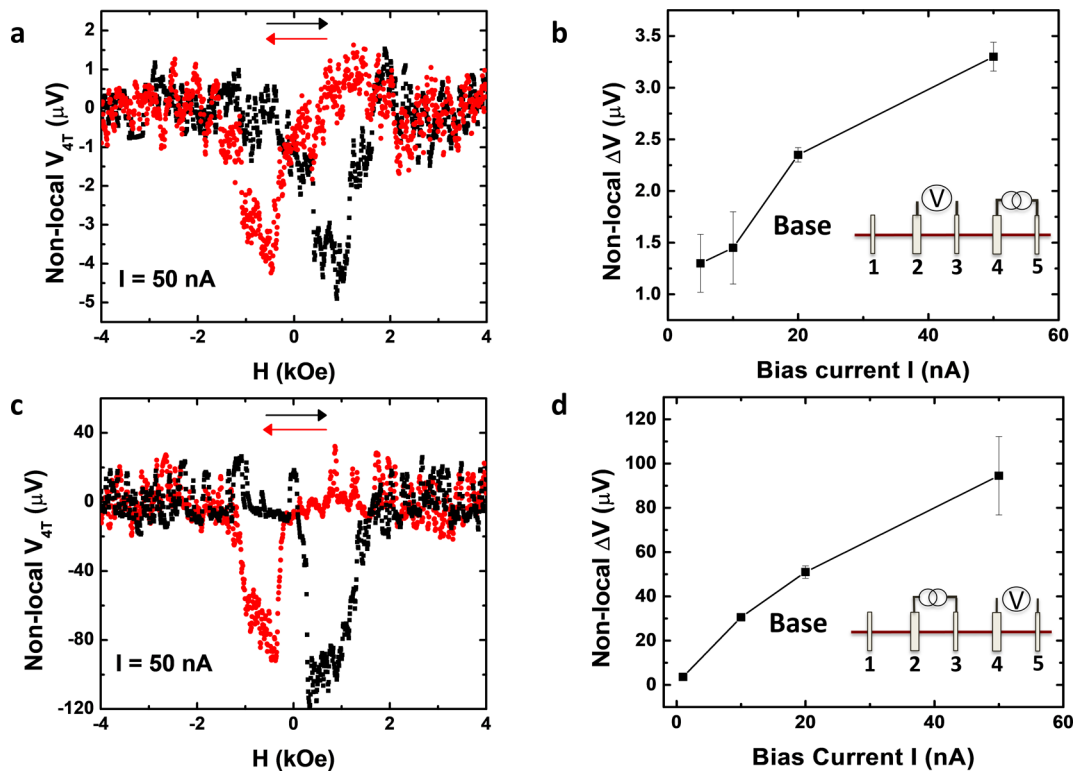


Figure 3. Nonlocal spin valve signals for the same Si NW channel upon exchanging injector and detector. NL-4T spin valve field sweeps at 5 K and bias current $I = 50$ nA and bias-dependence of their amplitude for the same Si NW section (between 3 and 4) but different spin injector-detector combinations: (a,b) #4 as injector and #3 as detector; (c,d) #3 as injector and #4 as detector. The contact resistances are $R_3 = 8$ k Ω and $R_4 = 41$ k Ω respectively. The error bars represent the standard deviation from the values extracted from two consecutive sweeps of the applied magnetic field.

tunneling mechanism now dominates the current flow due to the thin SB. The weakly insulating temperature dependence of the interfacial resistance $R_j(T)$, measured in the 3T configuration and shown in Figure S2c, further supports this conclusion.

The spin injection and detection experiments were performed on devices with $\text{Co}_{70}\text{Fe}_{30}$ electrodes of alternating widths. We focused primarily on low frequency (17 Hz) AC 2T and NL-4T spin valve measurements at 5 K. Figure 2a shows a schematic diagram of the device and the NL-4T measurement setup, Figure 2b shows a schematic diagram indicating the phosphorus doping gradient along the length of the Si NW, and Figure 2c–e show SEM micrographs of such a device. In the 2T configuration, two consecutive electrodes of different widths are used to apply electric current and measure the voltage, while in the NL-4T configuration the spin accumulation is measured outside the charge current path. In both cases, an in-plane magnetic field parallel to the long easy axis of the FM electrodes is swept, typically between -3000 Oe and $+3000$ Oe, while the spin valve voltage is measured. Figure 2f,g shows a set of representative 2T and NL-4T spin valve signals respectively for the same spin transport channel. For all the spin valve measurement results presented in this Letter, the background has been subtracted.

In the common lateral spin valve structures studied thus far, the spin transport channel is a uniform normal metal or semiconductor, and the spin injector and detector have identical FM/N interfaces. Our devices with an inhomogeneously doped Si NW channel and FM/NW contacts of varying resistances present a unique platform to investigate how the NL-4T signal depends on the injector, detector, and

channel properties. Specifically, on one and the same NW device, we can examine the variation of the NL-4T signal upon (i) interchanging the injector and detector between two neighboring FM/NW contacts of different properties, (ii) using a same FM/NW contact as the detector and the contact on either side as the injector.

Figure 3 shows a direct comparison of two NL-4T signals taken at 5 K from the same set of four FM/NW contacts on a Si NW, with the only difference being an interchange of the injector and detector between the two inner contacts, #3 and #4, across the same NW channel. The contact resistances are $R_3 = 8$ k Ω and $R_4 = 41$ k Ω . Figure 3a shows the NL-4T signal for the setup with #4 and #3 as injector and detector respectively at a bias current $I = 50$ nA, whereas Figure 3b shows the result after an interchange of the roles of the two electrodes. The two signals show broad similarities in their field dependences with approximately the same shape and switching fields for the spin valve voltages in the antiparallel states. This is consistent with the expectation that the field-dependence of the NL-4T voltage is determined by the relative magnetic orientations of the injector and detector. Two points are worth noting here. First, in contrast to the data in Figure 1f, the field sweeps here show less well-defined magnetic switchings. It is possible that a fully antiparallel alignment was not reached; however, that should not affect the comparison of the results in Figure 1a,c, because the same two electrodes were used as injector or detector. Second, the reference contacts used in our NL-4T measurements are ferromagnetic, which in principle could contribute to the spin-valve signals. However, in our devices they were located at distances at least twice the spin diffusion length. We did not

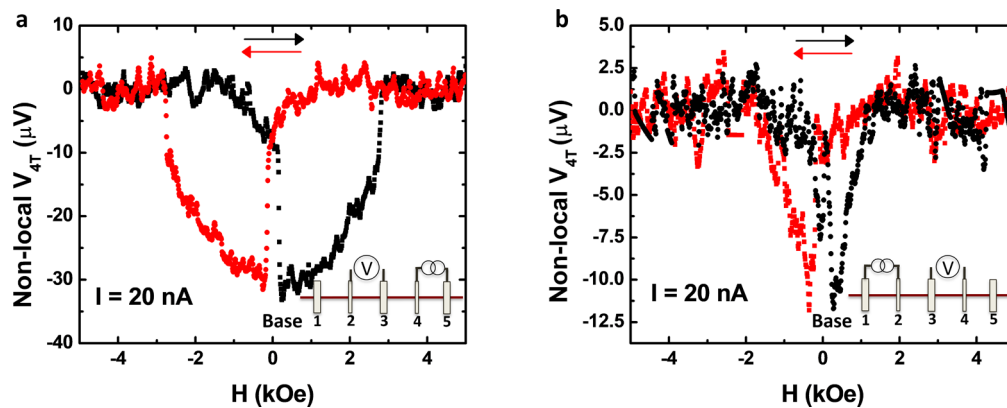


Figure 4. Nonlocal spin valve signals from the same detector and different injectors. (a,b) Background-subtracted 4T-NL spin valve signals from a Si NW device at 5 K. The bias current was $I = 20$ nA. The injection electrode was #4 and #2 respectively, whereas the detection electrode was the same (#3), as shown in the insets. The contact resistances are $R_2 = 25$ k Ω , $R_3 = 65$ k Ω , and $R_4 = 570$ k Ω .

observe multiple switchings in our NL-4T measurements, probably because our noise level was comparable to such small shifts. Notably, the amplitudes of the two signals differ by a factor of 26, at about 3.5 μ V (91.5 μ V) when the high (low) resistance contact #4 (#3) is used as the injector. We emphasize that the spin transport channels are the same section of the Si NW in both cases.

In Figure 4 we present data from a different set of NL-4T measurements: Here in one Si NW device, the same electrode is used for spin detection, while a different electrode on either side is used for spin injection. In both cases, the injection current is $I = 20$ nA, and the injector–detector distances are approximately the same, although the channels are two neighboring sections of the Si NW of different resistivities. Figure 4a (4b) shows the 4T-NL SV signal for the injector located on the more insulating (conducting) side of the NW with a signal amplitude of $\Delta V_{4T} = 20$ μ V ($\Delta V_{4T} = 9.2$ μ V).

These NL-4T spin-valve measurements using the FM/SC contacts of varying properties on the same NW provide a singular platform for reliably deciphering any correlation between the spin signal and FM/SC interface. The NL-4T signal is expected to be bipolar, depends on the relative orientation of the magnetizations of the injector and detector electrodes, and decays exponentially as the spins diffuse in the channel. In addition,⁴⁶ the spin accumulation signal (ΔR_S) depends on a host of material and device parameters including the contact, channel (SC) and FM resistances, R_i , R_N , and R_F , as well as the spin diffusion length in the SC. The general expression for ΔR_S can be approximated to simpler forms depending on whether the junctions are in the transparent, tunneling, or intermediate regime. In our case, $R_F \ll R_i < R_N$, places our devices in the intermediate regime of the Takahashi-Maekawa model that predicts⁴⁶

$$\Delta R_S = \frac{4P_J^2}{(1 - P_J^2)^2} \left(\frac{R_{i, \text{inj}} R_{2, \text{det}}}{R_N} \right) \frac{e^{-L/\lambda_N}}{1 - e^{-2L/\lambda_N}} \quad (1)$$

where R_i is the interface resistance of junction i , R_N is the spin resistance of the semiconductor channel, L and λ_N are the channel length and spin diffusion length, respectively. P_J is the interfacial current spin polarization of the injector and detector.

The Si NW channel resistances were determined directly from 4T IV measurements, and the FM/NW junction resistances were extracted in combination with 2T IV

measurements (the method is elaborated in [Supplementary Note 2](#)). In-depth examinations of the doping profile in such Si and Ge NWs by several different techniques,^{42–44} including a surface etching test,⁴³ revealed a core–shell structure of a core of uniform diameter and doping density and a thin shell of large gradients of thickness (10–1 nm) and doping density. To a good approximation, these NWs can be regarded as having constant mobility and diffusivity but significant variation in carrier density and electrical conductivity in the axial direction. In other words, we can think of the thin shell as a modulation doping layer, hence scattering of the electrons from the phosphorus dopants in the shell (relaxation due to hyperfine interaction with nuclei, at low temperatures) is homogenized once the spins are injected inside the channel. Therefore, we consider the spin diffusion length to be constant ($\lambda_N \approx 2.2$ μ m) in our Si NWs. This value is the average of the extracted spin diffusion lengths when we apply the theoretical model with fixed spin polarization from all different configurations, and they are consistent with values of $\lambda_N \approx 1.4$ μ m which were reported by spin transport experiments performed on non-degenerate Si with dopant concentration of about 2×10^{18} cm^{-3} at 300 K⁴⁷). In this study, we focus on the effects of interfacial properties on current spin polarization, and the specific value of the spin diffusion length does not affect the qualitative picture of that dependence. In our devices, this value is comparable to the channel length L (for all the spin valve configurations), as a result, for R_N we use the experimentally determined 4T resistance values. Specifically, the channel resistance for the device in Figure 3 is $R_N = 450$ k Ω (contacts 4–3), and for the device in Figure 4, $R_N = 276$ k Ω (contacts 3–2), and $R_N = 665$ k Ω (contacts 4–3). The corresponding channel lengths and resistivities are $L_{4-3} = 0.87$ μ m, $\rho_{4-3} = 0.122$ $\Omega\cdot\text{cm}$ (Figure 3), and $L_{3-2} = 1.77$ μ m, $\rho_{3-2} = 0.056$ $\Omega\cdot\text{cm}$, $L_{4-3} = 1.57$ μ m, $\rho_{4-3} = 0.175$ $\Omega\cdot\text{cm}$ (Figure 4). The spin polarization of the FM (CoFe) is taken as $P_J = 0.35$, which is a reasonable value for CoFe alloys.⁴⁸

Implicit in eq 1 is a symmetry between the injector and detector, which is in apparent contradiction with our results obtained on the device in Figure 3. In this configuration of NL-4T spin valve measurements across the same Si NW channel, interchanging the injector and detector is expected to yield identical spin valve signals, whereas in our device the spin accumulation ΔR_S is 26 times higher for the same injection current when the lower-resistance contact (#3) is used as the injector (Figure 3a,c). To account for possible effect of the bias

dependence of the spin injection efficiency,^{49,50} we measured the bias current dependence of the SV signals and observed a nonlinearity too small to be the origin of the observed injector–detector asymmetry. Furthermore, we compared directly the NL-4T spin valve signals in the two configurations at the same injector voltage bias of $V = 12$ mV, which are listed in Table 1, and they still differ by a factor of 15.6. Because the

Table 1. Sample Parameters and Spin Valve Results

sample	spin valve configuration ^a	R_i (k Ω) ^b	ΔR_S (Ω) ^c	α coefficient ^d
Figure 3	I 4–5; V 3–2 $V_{4,\text{inj}} = 12$ mV	$R_3: 8$	117	(#4) 0.25
	I 3–2; V 4–5 $V_{3,\text{inj}} = 12$ mV	$R_4: 41$	1830	(#3) 2.21
Figure 4		$R_2: 25$		
	I 4–5; V 3–2 $V_{4,\text{inj}} = 8$ mV	$R_3: 65$	2000	(#4) 0.12
	I 2–1; V 3–4 $V_{2,\text{inj}} = 8$ mV	$R_4: 570$	460	(#2) 0.27

^aThe spin valve configuration indicates which electrode is used as the spin injector. The voltage bias for the spin injectors is also provided. ^b R_i is the interface (contact) resistance. ^c $\Delta R_S = \Delta V/I$ is the nonlocal spin accumulation signal. ^dThe phenomenological parameter α describes how the injector polarization changes for different interfaces.

spin detector is unbiased in the NL configuration, these observations suggest that there is significant difference in interfacial injection current spin polarization depending on the nature of the FM/SC interface of the injector. Specifically, we observe that when the low resistance contact #3 is used as the injector, the spin accumulation signal is significantly higher, implying that a higher CoFe/Si NW contact resistance in our devices leads to a lower spin injection polarization.

A similar analysis can be applied to the data acquired with the device in Figure 4. In the two configurations in the experiment, the same junction (#3) is used as the spin detector, whereas junctions #2 and #4 are used as the spin injectors. Because the two injectors have different interface resistances and the two sections of the NW have different resistivities, the spin accumulation signals are expected to be different according to eq 1. Substituting the respective values for the interface resistance, channel resistance, and spin diffusion length $\lambda_N = 2.2$ μm into eq 1, if one assumes that the interfacial spin polarization P_j is the same for the injector and the detector, a ratio of 10.9 is expected for the spin accumulation signals, $\Delta R_S = \frac{\Delta V}{I}$

$$\text{ratio} = \frac{\Delta R_S (\text{high resistance injector})}{\Delta R_S (\text{low resistance injector})} = 10.9$$

However, the experimental data yield a ratio of 4.3, substantially lower than the theoretical expectation. We regard this as another strong indication that the higher resistance contact produces a lower spin injection polarization.

The experimental observations above point to a distinct correlation between the spin injection polarization and the varying doping density along the length of the NWs. To quantify the effect, we introduce a phenomenological parameter (α) in eq 1

$$\Delta R_S = \frac{4\alpha P_J^2}{(1 - \alpha P_J^2)^2} \left(\frac{R_{1,\text{inj}} R_{2,\text{det}}}{R_N} \right) \frac{e^{-L/\lambda_N}}{1 - e^{-2L/\lambda_N}}$$

The extracted values for the parameter α from the measurements in Figure 3 and Figure 4 are listed in Table 1. The parameter α is observed to decrease monotonically with increasing junction resistance R_i .

We interpret this variation of α with R_i as a systematic decrease of the injected current spin polarization across the FM/Si NW Schottky barrier of increasing width/height. From our earlier electrical characterization measurements with nonmagnetic (Ag) electrodes, we have observed a decrease of the Schottky barrier height with the increase of doping density.⁴⁵ As it has been shown theoretically and experimentally, the amplitude and even the sign of the spin polarization P can be dependent on the Schottky barrier height.⁵¹ Our explanation is within the picture of how the FM's 3d electronic states and 4sp electron states contribute to the tunneling current for varying Schottky junctions, and how the spin polarization and spin accumulation are affected.

As shown by scanning tunneling microscopy⁵² and spin-resolved superconducting tunneling,⁵³ both the highly spin polarized, more localized 3d electrons and the less polarized, highly mobile 4sp electrons contribute to the current from a transition metal FM across a tunnel barrier. The relative contributions of the two currents, thus the overall spin polarization of the current, depend on the interfacial bonding state between the FM and the barrier and the barrier height/thickness. These localized and delocalized currents have much different characteristic decay lengths k_{sp}^{-1} and k_{d}^{-1} , therefore their relative contributions to the current spin polarization can change greatly depending on the barrier thickness. Specifically, the total tunneling current can be expressed as the superposition of the 3d and 4sp tunneling currents

$$i_T = i_{\text{d},0} \exp(-k_{\text{d}}W) + i_{\text{sp},0} \exp(-k_{\text{sp}}W)$$

where $i_{\text{d},0}$, $i_{\text{sp},0}$ are the contributions to the tunneling current at the interface by the 3d and 4sp electrons, respectively, and W is the barrier width. The overall spin polarization of the tunneling current is given by $i_T P = i_{\text{d}} P_{\text{d}} + i_{\text{sp}} P_{\text{sp}}$. Importantly, in transition metal ferromagnets such as the CoFe, P_{d} is large and negative, whereas P_{sp} is small and positive. On oxide barriers such as Al_2O_3 , the interfacial bonding favors the 4sp states and the current spin polarization across the barrier is positive and increases with the barrier thickness due to the rapidly diminishing contribution from the negatively polarized 3d states.⁵³ In contrast, it was shown by STM experiments on AlGaAs⁵² that the tunneling current across the vacuum barrier is predominantly from the 3d states, hence the current spin polarization decreases with increasing barrier width.

In our experiments, we attribute the observed monotonic decay of the parameter α to the increased contribution of the 4sp states at increasing junction resistances. The effective polarization of the current across the junction can be expressed as

$$P = \frac{P_{\text{d}} + P_{\text{sp}} \frac{i_{\text{sp},0}}{i_{\text{d},0}} e^{-(k_{\text{sp}} - k_{\text{d}})W}}{1 + \frac{i_{\text{sp},0}}{i_{\text{d},0}} e^{-(k_{\text{sp}} - k_{\text{d}})W}} \approx P_{\text{d}} + P_{\text{sp}} \frac{i_{\text{sp},0}}{i_{\text{d},0}} e^{-(k_{\text{sp}} - k_{\text{d}})W} \quad (2)$$

This approximation holds for $(i_{\text{sp},0}/i_{\text{d},0})e^{(k_{\text{d}} - k_{\text{sp}})W} \ll 1$, which is valid for our devices, because $i_{\text{sp},0}/i_{\text{d},0} \approx 10^{-2}$ is

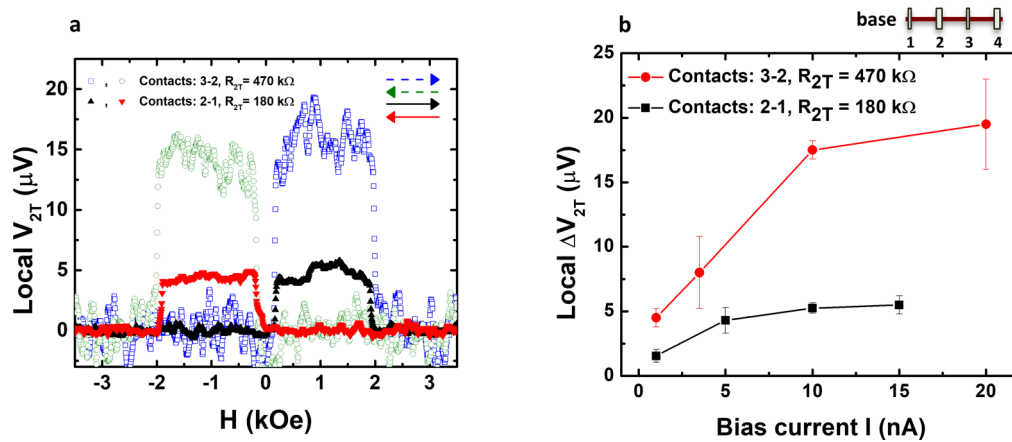


Figure 5. Two-terminal spin valve signals. (a) Background-subtracted local 2T spin valve signals at bias current $I = 10$ nA for two consecutive pairs of electrodes, 2–1 and 3–2, on the same NW with $R_{2T} = 180 \text{ k}\Omega$ and $R_{2T} = 470 \text{ k}\Omega$, respectively. (b) Bias current dependence of the 2T spin valve signals for the two electrode combinations. The error bars represent the standard deviation from the values extracted from two consecutive sweeps of the external magnetic field.

approximately the ratio of the 4sp to the 3d density of states at the Fermi level⁵² and the exponential factor is on the order of $e^{(k_d - k_{sp})W} \approx 10$ for relatively thin barriers.⁵³ Within this approximation, eq 2 indicates that the second term becomes larger as the depletion width (W) becomes wider, because $k_d > k_{sp}$. As a result, the overall current spin polarization decreases with increasing junction resistance (depletion width) because P_d and P_{sp} have opposite signs.

We now evaluate the Schottky barrier widths (W) in the CoFe/Si NW junctions and how they change (ΔW) along the Si NWs due to the doping gradient in our devices. In principle, the electrostatics and transport properties of NWs are modified due to the nanogeometries, especially the large surface-to-volume ratio. For example, the depletion width in ultrathin NWs may exhibit a stronger (exponential) dependence on the bias voltage and carrier density than the square root dependence in bulk junctions.⁵⁴ However, in the limit of R (radius of NW) $\gg W$ (depletion width), the expression reverts to the one for bulk semiconductors

$$W = \sqrt{\frac{2\epsilon V_{bi}}{eN_d}}$$

where V_{bi} is the built-in potential and N_d is the doping density. This expression for $V_{bi} = 0.85$ and 0.90 V and based on the estimated change of the effective carrier density from 6.8×10^{17} to $4.5 \times 10^{18} \text{ cm}^{-3}$ suggests a change in the depletion width from 40 to 16 nm. The built-in potential was calculated using the work function of cobalt ($\Phi_{Co} = 5.0$ eV) and the two effective carrier densities as doping densities. This estimate, however, does not take into account the core–shell structure of our Si NWs. It has been shown, by pulsed laser atom probe measurements, that the doping concentration of the shell can be more than an order of magnitude higher than the values extrapolated from the effective carrier densities.⁴² Additional potential profile studies support that most of the dopants in the shell are electrically active.⁴³ Therefore, the Schottky barrier width should be much thinner due to the much higher doping density in the shell. In such a case, one can estimate the depletion width to be $W \sim 3.6$ nm (for $V_{bi} = 0.98$ V and $N_d = 1 \times 10^{20} \text{ cm}^{-3}$), an order of magnitude thinner than the estimated values based on uniform doping. This range of depletion widths are consistent with the dominance of the 3d

states in the tunneling current, and a decrease of the overall current spin polarization with increasing W due to the increasing contribution of the oppositely polarized 4sp current

We also note that in some devices the spin-valve signals appear inverted. Theoretically, this is expected when the injection/detection polarizations have opposite signs. The inversion of the spin signals has been reported in Fe/GaAs heterostructures,⁵⁵ where the signal inversion were attributed to bias dependent effects. Our measurements are in the low bias regime, so we are inclined to believe that such effects are negligible. In our devices, it could originate from slight variations in the formation of the FM/SC contacts. A definitive understanding requires further studies.

We now turn our attention to the 2T spin valve measurements and how they compare with the NL-4T results. Figure 5a shows the background-subtracted 2T spin valve signals for two consecutive pairs of CoFe contacts on the same Si NW at the same injection current of 10 nA; the higher resistance pair produces a larger SV signal than the lower resistance pair. This is observed at all bias currents measured, as shown in Figure 5b. The ratio for the two signals is roughly $\Delta R_{3-2}/\Delta R_{2-1} \approx 3$. Equation 1 with the corresponding parameters for the two segments (Supporting Information Table S1) predicts a ratio of $\Delta R_{3-2}/\Delta R_{2-1} \approx 2.7$, which is in good agreement with the experimental result.

A direct comparison of the L-2T signals with the NL-4T signals provides additional insight into the spin transport. The three devices shown in Figures 3–5 enable such a comparison over a broad range of contact resistances. First, we note that in all cases for any pair of injector and detector similar switching fields are observed for both L-2T and NL-4T measurement schemes (e.g., Figure 1f,g), which is a strong indicator that the L-2T signals indeed originate from the spin accumulation in the Si NW channel and not from spurious effects such as the magneto-Coulomb effect,⁵⁶ local Hall effects,⁵⁷ and anisotropic magnetoresistance effects. In spin valves, the ratio of the 2T and NL-4T spin valve signal amplitudes, $\Delta V_{2T}/\Delta V_{4T}$, is predicted to be two in a one-dimensional spin diffusion model.^{32,58} In our case, this ratio varies greatly, from being close to two to values significantly larger, depending on the positions of the injector/detector electrodes on the Si NW, and more sensitively, on the choice of the injector and detector in

the NL-4T measurement. The most dramatic example is on the device shown in Figure 3. For the same bias current, $I = 10$ nA, the NL-4T signals across the same NW segment (between #3 and #4) from the combinations $I, 3, 2$; $V, 4, 5$ and $I, 4, 5$; $V, 3, 2$ are $25.8 \mu\text{V}$ and $1.4 \mu\text{V}$, respectively. The local 2T signal between 3 and 4 is $57 \mu\text{V}$, corresponding to ratios of $\Delta V_{2T}/\Delta V_{4T} = 2.2$ and 41 . The variations arise predominantly from the different interfacial properties of the two adjacent FM/SC contacts due to the axial doping gradient, while the different widths of the FM electrodes play a much lesser role. This discrepancy can be associated with the previous results from the spin diffusion model, where the spin injection polarization was higher for the low resistance junction. For a symmetric device, at low bias the 2T signal is expected to be equal to the sum of the two signals measured in the nonlocal configuration for the same transport channel,⁵⁹ $\Delta V_{2T} = \Delta V_{i,j}^{\text{NL}} + \Delta V_{j,i}^{\text{NL}}$, where i, j correspond to the different junctions, and $\Delta V_{i,j}^{\text{NL}}$ correspond to the voltage drop at contact i due to the spin accumulation generated at contact j . In our case, this relation does not hold; $\Delta V_{4,3}^{\text{NL}} + \Delta V_{3,4}^{\text{NL}} = 25.8 + 1.4 \mu\text{V} = 27.2 \mu\text{V}$, while the 2T signal is 2.1 times as large. One possible reason for this discrepancy is the effect of drift on spin diffusion. It is known that an electric field can affect spin transport along the channel, and effectively modify spin diffusion lengths by enhancing or suppressing the diffusion process of the spins.⁵⁹ In our case, we observe an enhancement in the 2T signal.

In conclusion, we have examined the important role of the nanoscopic FM/SC interface on spin injection in Si NWs with an inherent axial doping gradient. This unique material characteristic translates into a systematic variation of the FM/Si NW contacts of Schottky nanojunctions of different barrier width/height along the length of an individual Si NW. Spin valve measurements with different combinations of the FM electrodes on the same Si NW reveal a distinct anticorrelation between the injected current spin polarization and the FM/Si NW junction resistance. We ascribe the observations to the variation of the relative contributions of the differently and oppositely spin polarized 3d states and 4sp states in the FM to the injection current. These devices are good candidates for studying the control of the interface spin polarization with different Schottky barrier heights without having to use different FM materials of different work functions, which has been studied in FM/Si interfaces⁶⁰ or by using different oxide layer thicknesses as tunnel barriers.⁶¹ Practically, our experiments on this device platform demonstrate that there is an optimal window of interface parameters for maximum spin injection efficiency and current spin polarization, and the possibility of using asymmetric interfaces to acquire higher spin signals because different contact profiles result in different spin injection/extraction polarizations.

Experimental Methods. The silicon nanowires used in this experiment are n-type phosphorus doped and they are grown on SiO₂ substrates via the vapor–liquid–solid (VLS) deposition method. The wafers were coated with 4 nm of gold via thermal evaporation prior to the growth process. The growth took place in a chemical vapor deposition (CVD) system at 460 °C for a period of 15 min by a gas flow of silane (SiH₄) at a rate of 80 sccm and 20 Torr of reaction pressure. Silane is used as the precursor gas to create Au–Si alloy droplets on the wafer surface, which act as a catalyst. Phosphorus doping was achieved by simultaneously introducing phosphine gas (PH₃) inside the growth chamber at a flow rate of 12 sccm. Upon completion of the growth, the Si NWs

are suspended in isopropanol solution via sonication. The diameter of each individual NW, between the tip (gold droplet) and the base, ranges from 90 to 140 nm and the length 25–30 μm .

■ ASSOCIATED CONTENT

Supporting Information

The Supporting Information is available free of charge on the ACS Publications website at DOI: 10.1021/acs.nanolett.8b01423.

Additional experimental details. Figures showing SEM micrographs of a Si NW, electrical characterization measurements and I – V characteristics, contact resistance calculation method, interface and channel parameters, and description of doping gradient profile (PDF)

■ AUTHOR INFORMATION

Corresponding Author

*E-mail: (P.X.) pxiong@fsu.edu.

ORCID

Konstantinos Kountouriotis: 0000-0001-9204-7401

Jorge L. Barreda: 0000-0001-9816-9389

Peng Xiong: 0000-0003-1746-1404

Author Contributions

K.K. and P.X. conceived the experiments and interpreted the data. K.K. performed the electrical transport measurements, spin transport measurements, SEM measurements and analyzed the data. J.B., T.K., and M.Z. synthesized the Si nanowires. The manuscript was written by K.K. and P.X. with inputs from other authors.

Notes

The authors declare no competing financial interest.

■ ACKNOWLEDGMENTS

This research was funded by NSF under contract DMR-1308613. We thank Stephan von Molnár and David Van Winkle for fruitful discussions.

■ REFERENCES

- (1) Datta, S.; Das, B. Electronic analog of the electro-optic modulator. *Appl. Phys. Lett.* **1990**, *56*, 665.
- (2) Fabian, J.; Žutić, I.; Das Sarma, S. Theory of spin-polarized bipolar transport in magnetic n -junctions. *Phys. Rev. B: Condens. Matter Mater. Phys.* **2002**, *66*, 165301.
- (3) Monsma, D. J.; Lodder, J. C.; Popma, T. J.; Dieny, B. Perpendicular hot electron spin-valve effect in a new magnetic field sensor: The spin-valve transistor. *Phys. Rev. Lett.* **1995**, *74*, 5260–5263.
- (4) Žutić, I.; Fabian, J.; Das Sarma, S. Spintronics: Fundamentals and applications. *Rev. Mod. Phys.* **2004**, *76*, 323–410.
- (5) Fabian, J.; Matos-Abiague, A.; Ertler, C.; Stano, P.; Žutić, I. Semiconductor spintronics. *Acta Phys. Slovaca* **2007**, *57*, 565.
- (6) Zhu, H. J.; et al. Room-temperature spin injection from Fe into GaAs. *Phys. Rev. Lett.* **2001**, *87*, 016601.
- (7) Hanbicki, A. T.; Jonker, B. T.; Itskos, G.; Kioseoglou, G.; Petrou, A. Efficient electrical spin injection from a magnetic metal/tunnel barrier contact into a semiconductor. *Appl. Phys. Lett.* **2002**, *80*, 1240–1242.
- (8) Van Dorpe, P.; Van Roy, W.; Moutsny, V. F.; Borghs, G.; De Boeck, J. Efficient electrical spin injection in GaAs: A comparison between AlOx and Schottky injectors. *J. Vac. Sci. Technol., A* **2004**, *22*, 1862–1867.

- (9) Jonker, B. T.; Kioseoglou, G.; Hanbicki, A. T.; Li, C. H.; Thompson, P. E. Electrical spin-injection into silicon from a ferromagnetic metal/tunnel barrier contact. *Nat. Phys.* **2007**, *3*, 542–546.
- (10) Lou, X.; et al. Electrical detection of spin transport in lateral ferromagnet-semiconductor devices. *Nat. Phys.* **2007**, *3*, 197–202.
- (11) Koo, H. C.; et al. Control of Spin Precession in a Spin-Injected Field Effect Transistor. *Science* **2009**, *325*, 1515.
- (12) Han, W.; et al. Spin injection and detection in lanthanum- and niobium-doped SrTiO₃ using the Hanle technique. *Nat. Commun.* **2013**, *4*, 2134.
- (13) Oltcher, M.; et al. Electrical spin injection into high mobility 2D systems. *Phys. Rev. Lett.* **2014**, *113*, 236602.
- (14) Chuang, P.; et al. All-electric all-semiconductor spin field-effect transistors. *Nat. Nanotechnol.* **2015**, *10*, 35.
- (15) Chang, L. T.; et al. Electrical detection of spin transport in Si two-dimensional electron gas systems. *Nanotechnology* **2016**, *27*, 365701.
- (16) Schmidt, G.; Ferrand, D.; Molenkamp, L. W.; Filip, A. T.; van Wees, B. J. Fundamental obstacle for electrical spin injection from a ferromagnetic metal into a diffusive semiconductor. *Phys. Rev. B: Condens. Matter Mater. Phys.* **2000**, *62*, R4790–R4793.
- (17) Fert, A.; Jaffrès, H. Conditions for efficient spin injection from a ferromagnetic metal into a semiconductor. *Phys. Rev. B: Condens. Matter Mater. Phys.* **2001**, *64*, 184420.
- (18) Kioseoglou, G.; et al. Electrical spin injection into Si: A comparison between Fe/Si Schottky and Fe/Al₂O₃ tunnel contacts. *Appl. Phys. Lett.* **2009**, *94*, 122106.
- (19) Jansen, R. Electrical spin injection into moderately doped silicon enabled by tailored interfaces. *Phys. Rev. B: Condens. Matter Mater. Phys.* **2010**, *82*, 241305.
- (20) Wu, M. W.; Jiang, J. H.; Weng, M. Q. Spin dynamics in semiconductors. *Phys. Rep.* **2010**, *493*, 61–236.
- (21) Kiselev, A. A.; Kim, K. W. Progressive suppression of spin relaxation in two-dimensional channels of finite width. *Phys. Rev. B: Condens. Matter Mater. Phys.* **2000**, *61*, 13115–13120.
- (22) Mal'shukov, A. G.; Chao, K. A. Waveguide diffusion modes and slowdown of D'yakonov-Perel' spin relaxation in narrow two-dimensional semiconductor channels. *Phys. Rev. B: Condens. Matter Mater. Phys.* **2000**, *61*, R2413–R2416.
- (23) Balandin, A. A. Nanophonics: Phonon Engineering in Nanostructures and Nanodevices. *J. Nanosci. Nanotechnol.* **2005**, *5*, 1015–1022.
- (24) Holleitner, A. W.; Sih, V.; Myers, R. C.; Gossard, A. C.; Awschalom, D. D. Suppression of spin relaxation in submicron InGaAs wires. *Phys. Rev. Lett.* **2006**, *97*, 036805.
- (25) Tang, J.; et al. Electrical Spin Injection and Detection in Mn₅Ge₃/Ge/Mn₅Ge₃ Nanowire Transistors. *Nano Lett.* **2013**, *13*, 4036–4043.
- (26) Heedt, S.; et al. Electrical Spin Injection into InN Semiconductor Nanowires. *Nano Lett.* **2012**, *12*, 4437–4443.
- (27) van 't Erve, O. M. J.; et al. *Nat. Commun.* **2015**, *6*, 7541.
- (28) Tarun, J.; et al. Demonstration of spin valve effects in silicon nanowires. *J. Appl. Phys.* **2011**, *109*, 07C508.
- (29) Liu, E.-S.; Nah, J.; Varshneyan, K. M.; Tutuc, E. Lateral Spin Injection in Germanium Nanowires. *Nano Lett.* **2010**, *10*, 3297–3301.
- (30) Zhang, S.; et al. Electrical Spin Injection and Detection in Silicon Nanowires through Oxide Tunnel Barriers. *Nano Lett.* **2013**, *13*, 430–435.
- (31) Johnson, M.; Silsbee, R. H. Interfacial charge-spin coupling: Injection and detection of spin magnetization in metals. *Phys. Rev. Lett.* **1985**, *55*, 1790–1793.
- (32) Jedema, F. J.; Nijboer, M. S.; Filip, A. T.; van Wees, B. J. Spin injection and spin accumulation in all-metal mesoscopic spin valves. *Phys. Rev. B: Condens. Matter Mater. Phys.* **2003**, *67*, 085319.
- (33) Appelbaum, I.; Huang, B.; Monsma, D. J. Electronic measurement and control of spin transport in silicon. *Nature* **2007**, *447*, 295–298.
- (34) Jansen, R. Silicon spintronics. *Nat. Mater.* **2012**, *11*, 400–408.
- (35) Sasaki, T.; et al. Temperature dependence of spin diffusion length in silicon by Hanle-type spin precession. *Appl. Phys. Lett.* **2010**, *96*, 122101.
- (36) Ando, Y.; et al. Electrical injection and detection of spin-polarized electrons in silicon through an Fe₃Si/Si Schottky tunnel barrier. *Appl. Phys. Lett.* **2009**, *94*, 182105.
- (37) Dash, S. P.; Sharma, S.; Patel, R. S.; de Jong, M. P.; Jansen, R. Electrical creation of spin polarization in silicon at room temperature. *Nature* **2009**, *462*, 491–494.
- (38) Gray, N. W.; Tiwari, A. Room temperature electrical injection and detection of spin polarized carriers in silicon using MgO tunnel barrier. *Appl. Phys. Lett.* **2011**, *98*, 102112.
- (39) Li, C. H.; van 't Erve, O. M.; Jonker, B. T. Electrical injection and detection of spin accumulation in silicon at 500 K with magnetic metal/silicon dioxide contacts. *Nat. Commun.* **2011**, *2*, 245.
- (40) Hanbicki, A. T.; et al. Analysis of the transport process providing spin injection through an Fe/AlGaAs Schottky barrier. *Appl. Phys. Lett.* **2003**, *82*, 4092–4094.
- (41) Liu, T.; Liang, R.; Okoli, O.; Zhang, M. Fabrication of silicon nanowire on freestanding multiwalled carbon nanotubes by chemical vapor deposition. *Mater. Lett.* **2015**, *159*, 353–356.
- (42) Perea, D. E.; et al. Direct measurement of dopant distribution in an individual vapour-liquid-solid nanowire. *Nat. Nanotechnol.* **2009**, *4*, 315–319.
- (43) Allen, J. E.; Perea, D. E.; Hemesath, E. R.; Lauhon, L. J. Nonuniform Nanowire Doping Profiles Revealed by Quantitative Scanning Photocurrent Microscopy. *Adv. Mater.* **2009**, *21*, 3067–3072.
- (44) Schlitz, R. A.; Perea, D. E.; Lensch-Falk, J. L.; Hemesath, E. R.; Lauhon, L. J. Correlating dopant distributions and electrical properties of boron-doped silicon nanowires. *Appl. Phys. Lett.* **2009**, *95*, 162101.
- (45) Barreda, J. L.; Keiper, T. D.; Zhang, M.; Xiong, P. Multiple Schottky Barrier-Limited Field-Effect Transistors on a Single Silicon Nanowire with an Intrinsic Doping Gradient. *ACS Appl. Mater. Interfaces* **2017**, *9*, 12046–12053.
- (46) Takahashi, S.; Maekawa, S. Spin injection and detection in magnetic nanostructures. *Phys. Rev. B: Condens. Matter Mater. Phys.* **2003**, *67*, 052409.
- (47) Sasaki, T.; et al. Local magnetoresistance in Fe/MgO/Si lateral spin valve at room temperature. *Appl. Phys. Lett.* **2014**, *104*, 052404.
- (48) Soulen, R. J.; et al. Measuring the Spin Polarization of a Metal with a Superconducting Point Contact. *Science* **1998**, *282*, 85.
- (49) Ciorga, M. Electrical spin injection and detection in lateral all-semiconductor devices. *Phys. Rev. B: Condens. Matter Mater. Phys.* **2009**, *79*, 165321.
- (50) Peterson, T.; et al. Spin injection and detection up to room temperature in Heusler alloy/n-GaAs spin valves. *Phys. Rev. B: Condens. Matter Mater. Phys.* **2016**, *94*, 235309.
- (51) Smith, D. L.; Ruden, P. P. Spin-polarized tunneling through potential barriers at ferromagnetic metal/semiconductor Schottky contacts. *Phys. Rev. B: Condens. Matter Mater. Phys.* **2008**, *78*, 125202.
- (52) Alvarado, S. F. Tunneling Potential Barrier Dependence of Electron Spin Polarization. *Phys. Rev. Lett.* **1995**, *75*, 513–516.
- (53) Münzenberg, M.; Moodera, J. S. Superconductor-ferromagnet tunneling measurements indicate $s\text{-}p$ -spin and $d\text{-}s$ -spin currents. *Phys. Rev. B: Condens. Matter Mater. Phys.* **2004**, *70*, 060402.
- (54) Léonard, F.; Talin, A. A. Electrical contacts to one- and two-dimensional nanomaterials. *Nat. Nanotechnol.* **2011**, *6*, 773.
- (55) Crooker, S. A. Bias-controlled sensitivity of ferromagnet/semiconductor electrical spin detectors. *Phys. Rev. B: Condens. Matter Mater. Phys.* **2009**.
- (56) van der Molen, S. J.; Tombros, N.; van Wees, B. J. Magneto-Coulomb effect in spin-valve devices. *Phys. Rev. B: Condens. Matter Mater. Phys.* **2006**, *73*, 220406.
- (57) Monzon, F. G.; Patterson, D. S.; Roukes, M. L. Characterization of individual nanomagnets by the local Hall effect. *J. Magn. Magn. Mater.* **1999**, *195*, 19–25.

(58) Jaffrès, H.; George, J. M.; Fert, A. Spin transport in multiterminal devices: Large spin signals in devices with confined geometry. *Phys. Rev. B: Condens. Matter Mater. Phys.* **2010**, *82*, 140408.

(59) Oltcher, M.; et al. Gate-tunable large magnetoresistance in an all-semiconductor spin valve device. *Nat. Commun.* **2017**, *8*, 1807.

(60) Min, B.-C.; Motohashi, K.; Lodder, C.; Jansen, R. Tunable spin-tunnel contacts to silicon using low-work-function ferromagnets. *Nat. Mater.* **2006**, *5*, 817–822.

(61) Lu, Y.; et al. MgO thickness dependence of spin injection efficiency in spin-light emitting diodes. *Appl. Phys. Lett.* **2008**, *93*, 152102.